Appl. Phys. B 72, 921–925 (2001) / Digital Object Identifier (DOI) 10.1007/s003400100588

Applied Physics B
Lasers
and Optics

Dual spectral filters with multi-layered grating waveguide structures

G. Levy-Yurista*, A.A. Friesem

Department of Physics of Complex Systems, Weizmann Institute of Science, Rehovot 76100, Israel

Received: 14 December 2000/Published online: 9 May 2001 –

Abstract. Promising configurations for dual spectral filters based upon grating-waveguide structures are presented. In these configurations, the parameters of the multimode waveguide and grating are carefully chosen to achieve dual resonances at two different pre-determined wavelengths. Specifically, the grating-waveguide structure resonates for each pre-selected wavelength with a different waveguide mode. Theoretical and experimental results reveal that the resonance wavelengths can be accurately selected and that the resonance spectral bandwidths can be less than 1 nm with high contrast ratios.

PACS: 42.25.Fx; 42.79.Ci; 42.79.Dj

Optical filters based upon diffraction anomalies from gratings have been extensively investigated for many years. The diffraction anomaly phenomenon was first investigated by Wood [1], who observed very strong variations in the intensity of the diffracted spectral orders over narrow frequency bands. Wood's observation was followed by numerous theoretical and experimental investigations that dealt with the resonance behavior in reflection gratings [2–8]. These investigations have been expanded to resonance anomalies in grating–waveguide structures (GWS) and have included new theoretical and experimental developments [9–18]. In general, filters based on GWS are designed to reflect the incoming light at one specific wavelength. Indeed, extremely narrow resonance bandwidths on the order of 0.1 nm have been obtained [19, 20]. Here we present an advanced GWS design and fabrication procedures which enable the selection of two pre-determined resonance wavelengths. We show that it is possible to accurately control each of the resonance wavelengths, so as to obtain two simultaneous filters, thereby extending the range of applications of GWS.

*Corresponding author.
(Fax: +972-8/934-4109, E-mail: feguy@wisemail.weizmann.ac.il)

1 Basic principles of GWS

The basic configuration of a GWS is schematically shown in Fig. 1. It is composed of a thin dielectric or semiconductor waveguide layer and an additional transparent layer in which a grating is formed. Below these is a substrate and above is a superstrate. When such a GWS is illuminated with an incident light beam, most of the beam is directly transmitted, while the rest is diffracted, trapped in the waveguide layer and subsequently partially rediffracted outwards. At a specific resonant wavelength and angular orientation of the incident beam, the rediffracted beam interferes destructively with the transmitted beam, so that the incident beam is completely reflected from the GWS. In general, the resonance bandwidths are limited by the losses that are caused by material and fabrication defects.

In the most basic form, the resonance wavelength λ_0 in GWS is related to the grating period Λ as follows:

$$n_{\mathrm{sp}} k \sin\theta + mK(\Lambda) = n_{\mathrm{wg}} k(\lambda_0)\cos\psi\,, \tag{1}$$

where n_{sp} is the refractive index of the superstrate layer above the structure, n_{wg} is the refractive index of the waveguide layer, and θ and ψ are the angle of incident light and the angle of diffracted light, respectively, as shown in Fig. 1. $k = 2\pi/\lambda_0$ is the light wavevector at resonance, $K = 2\pi/\Lambda$ the grating wavevector, and m an integer ($m = 1, 2, 3, \ldots$) where $m = 1$ is used in the simplest case of a single-mode waveguide. Following Tien and Ulrich [21], we derive an implicit equation to relate waveguide thickness W and grating period Λ, assuming the thin grating approximation, as

$$Wn_{\mathrm{wg}} k \sin\psi(\Lambda) = \Phi_{\mathrm{sb}}(\Lambda) + \Phi_{\mathrm{sp}}(\Lambda) + (m-1)\pi\,, \tag{2}$$

where $\psi(\Lambda)$ is a function of the period Λ in accordance with (1) and $\Phi_{\mathrm{sb}}(\Lambda)$ and $\Phi_{\mathrm{sp}}(\Lambda)$ are the phases accumulated by the waves trapped in the waveguide each time they are totally internally reflected from the waveguide–substrate and waveguide–superstrate surfaces, respectively. The phases Φ_{sb}

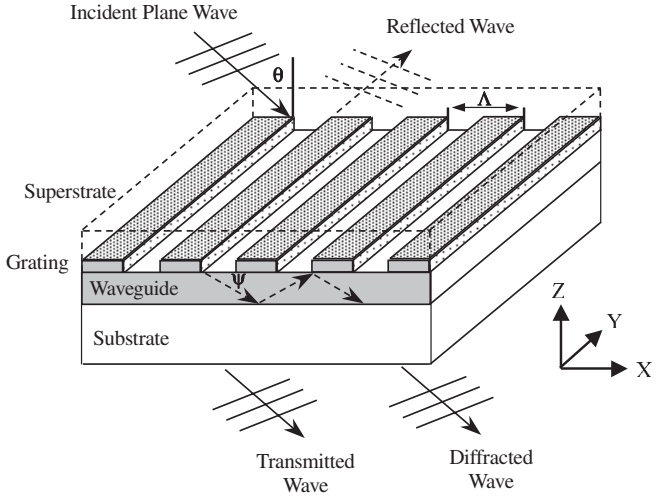

Fig. 1. Basic configuration of a grating–waveguide structure (GWS)

and Φ_{sp} for the TE modes are given by [21]:

$$\Phi_i^{(TE)}(\Lambda) = \arctan\left(\frac{\sqrt{\left[n_{wg}\cos\psi(\Lambda)\right]^2 - n_i^2}}{n_{wg}\sin\psi(\Lambda)}\right), \quad (3)$$

where $i = sb$ or $i = sp$ for the substrate-related phase or the superstrate-related phase, respectively. For the TM modes, these phases are,

$$\Phi_i^{(TM)}(\Lambda) = \arctan\left(\frac{n_{wg}^2}{n_i^2}\cdot\frac{\sqrt{\left[n_{wg}\cos\psi(\Lambda)\right]^2 - n_i^2}}{n_{wg}\sin\psi(\Lambda)}\right). \quad (4)$$

Solving (2), using (1) and (3) for the TE modes [or using (1) and (4) for the TM modes], yields, for a thin grating approximation, the grating period Λ as a function of the waveguide thickness W, for a specific GWS resonance wavelength λ_0. Accordingly, for a specific resonance wavelength, there could be many choices of pairs of waveguide thickness W and grating period Λ. Moreover, for a multimode waveguide the incident light can be coupled to a higher-order mode of the waveguide, i.e., $m \geq 1$, thus increasing the range of choices of such Λ and W pairs for a specific resonance wavelength.

As an example, we calculated the grating period as a function of waveguide thickness, for a waveguide that can support three modes and for the two different resonance wavelengths of 1530 nm and 1567 nm. For these calculations we assumed a GWS configuration in which the waveguide and grating layers are formed with InGaAsP ($n = 3.391$) and the substrate and superstrate layers are formed with InP ($n = 3.17$). The light is assumed to be normal incident. The results are presented in Fig. 2. The solid curves give the results for the three lowest modes at the resonance wavelength 1530 nm, whereas the dashed curves are for the three lowest modes at the resonance wavelength 1567 nm.

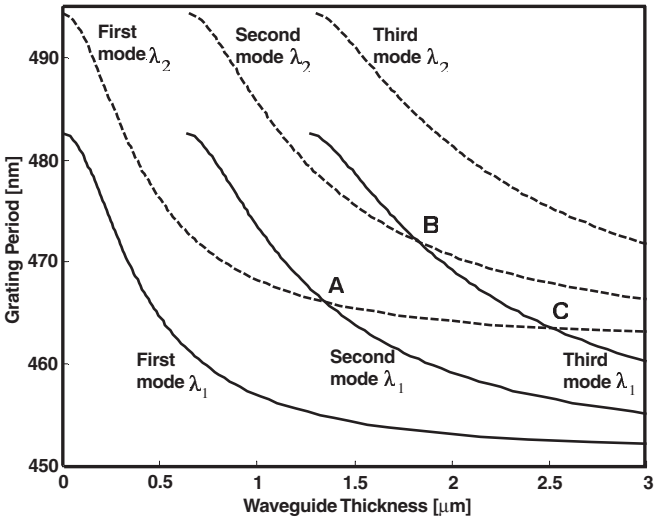

Fig. 2. Grating period Λ as a function of waveguide thickness W for the three lowest modes in a GWS at two different wavelengths. *Solid curves*: $\lambda_1 = 1530$ nm; *dashed curves*: $\lambda_2 = 1567$ nm. *Intersection points* A, B and C: different solutions for a double resonance GWS operation at λ_1 and λ_2

2 Design of a double-resonance GWS

We now consider how to design a single GWS that can simultaneously have two resonance wavelengths. From the results shown in Fig. 2, it is evident that there are many values of grating period and waveguide thickness pairs that would satisfy a specific resonance wavelength. We can exploit this redundancy in oder to obtain a particular choice of grating period Λ and waveguide thickness W pair that fits two specific resonance wavelengths.

The procedure for obtaining the values of grating period and waveguide thickness pairs for a GWS of two specific resonance wavelengths λ_1 and λ_2 involves several steps. In the first step we calculate the grating period as a function of waveguide thickness for several modes of one specific resonance wavelength, λ_1. Next, we repeat the calculations for the other specific resonance wavelength, λ_2. These calculations provide results similar to these shown in Fig. 2, where for each resonance wavelength we obtain a set of curves that relate the grating period to the waveguide thickness.

The intersection points of the curves of the first resonance wavelength λ_1 with the curves of the second resonance wavelength λ_2 determine the values of grating period and waveguide thickness pairs that satisfy both resonance wavelengths. Note that the incident light at each resonance wavelength is coupled to a different waveguide mode.

To illustrate our procedure, we refer to the results depicted in Fig. 2. Here, the intersection points A, B and C denote different pair values of grating period and waveguide thickness that would result in a GWS with two resonance wavelengths. Specifically, the intersection point A corresponds to a waveguide thickness of 1.35 μm and a grating period of 466 nm. For these values, the grating couples the incident light to the second mode of the waveguide at a resonance wavelength of $\lambda_1 = 1530$ nm and to the first mode of the waveguide at $\lambda_2 = 1567$ nm. Similarly, intersection point B corresponds to coupling of the incident light to the third waveguide mode at λ_1 and to the second waveguide mode at λ_2. Intersection point C corresponds to coupling the incident light to the third waveguide mode at λ_1 and to the first waveguide mode at λ_2. All the calculations were performed for normal incidence.

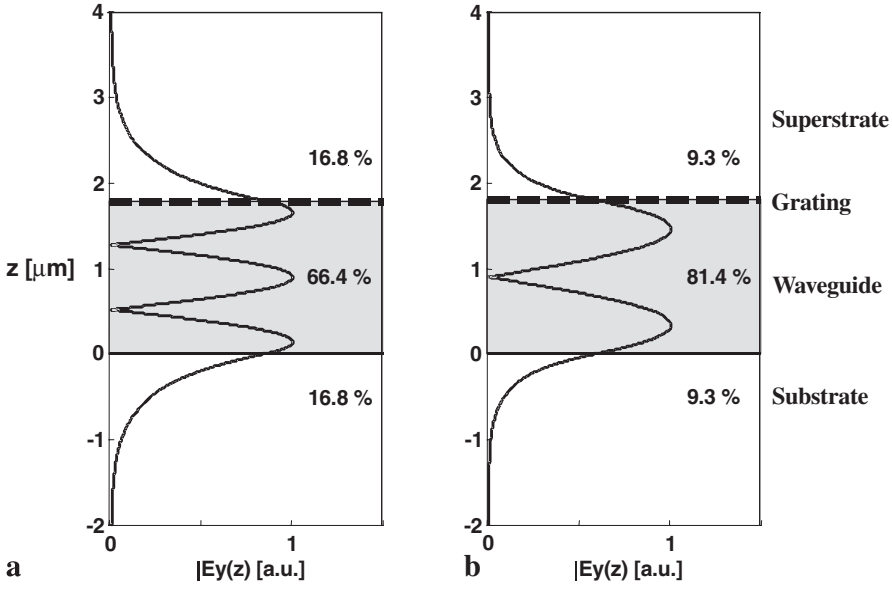

Fig. 3a,b. Absolute value of the modal field distribution of a double-resonance GWS corresponding to intersection point B in Fig. 2. **a** Third-mode absolute amplitude distribution for $\lambda_1 = 1530$ nm; **b** Second-mode absolute amplitude distribution for $\lambda_2 = 1567$ nm. The fractional mode amplitude in each region of the GWS is marked by a percent of the total mode amplitude

We also calculated the absolute value of the modal field distribution in the GWS for the two different resonance wavelengths: $\lambda_1 = 1530$ nm and $\lambda_2 = 1567$ nm. Representative results with grating period and waveguide thickness values corresponding to intersection point B in Fig. 2, are presented in Fig. 3. The grating period is $\Lambda = 472.2$ nm and the waveguide thickness $W = 1.8$ μm. Figure 3a shows the absolute value of the amplitude distribution of the third mode into which the incident light is coupled at λ_1. Figure 3b shows the absolute value of the amplitude distribution of the second mode into which the incident light is coupled at λ_2. The fractional mode amplitude in each region of the GWS is marked by a percent of the total amplitude of the mode. Since each mode spreads differently in the waveguide and surrounding layers, there is a different grating coupling coefficient for each mode. This, in turn, results in a different resonance spectral bandwidth. As evident from Fig. 3 the confinement of the second mode, associated with λ_2, is stronger than that of the third mode, associated with λ_1, in the waveguide region. This, in turn, leads to a lower interaction of the mode with the grating, so as to obtain a narrower spectral resonance bandwidth at λ_2.

3 Fabrication of a double-resonance GWS

We designed and fabricated several GWSs, each having two different specific resonance wavelengths. For their fabrication we used the GWS geometric configuration schematically shown in Fig. 4, in which the grating layer is not directly adjacent to the waveguide layer [20]. The advantages of such a configuration over that in which the grating is etched into the waveguide layer include lower losses and better control of the layer's thickness during fabrication. The grating period and waveguide thickness required for each GWS were first determined in accordance with the thin grating approximation described above, and these were then more accurately determined by resorting to a numerical algorithm based on the exact eigenfunction approach and Maxwell's equation [22] to obtain a higher-order correction. In general we found that the higher-order corrections required were minor. For example,

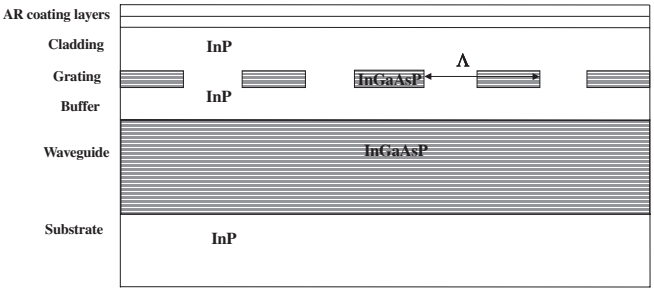

Fig. 4. Experimental GWS configuration for double-resonance wavelengths

the calculated spectral response for the double-resonance GWS configuration, fabricated with the set of parameter values of intersection point B, is shown in Fig. 5. Here we show the normalized reflected intensity as a function of wavelength when the incident beam was TE polarized. The calculated spectral resonance bandwidths at FWHM are 0.17 nm and 0.08 nm for λ_1=1530 nm and λ_2=1567 nm, respectively.

For the fabrication of the GWS corresponding to intersection point B in Fig. 2, we started with an InP substrate on which we deposited using metal–organic chemical-vapor deposition (MOCVD), an intrinsic InP layer with a thickness of 200 nm, followed by an InGaAsP waveguide layer with a thickness of 1750 nm. Next, we deposited a shallow buffer layer of InP with a thickness of 10 nm, again using MOCVD. Next, we deposited another intrinsic InGaAsP layer with a thickness of 100 nm, which was etched to form the grating layer. This grating layer was formed by first using an electron beam to expose a PMMA photoresist that was coated on top of the layer, which was then etched by means of the selective reactive-ion etching process. The duty cycle of the grating was controlled by the electron beam exposure and was chosen to be 50%, with a grating period of 472.2 nm. The etching process was designed to stop at the InP buffer layer. Then, again using MOCVD, a final InP superstrate layer was regrown on top of the etched structure up to a thickness of 1300 nm. The surface roughness resulting from the etching process was thus eliminated al-

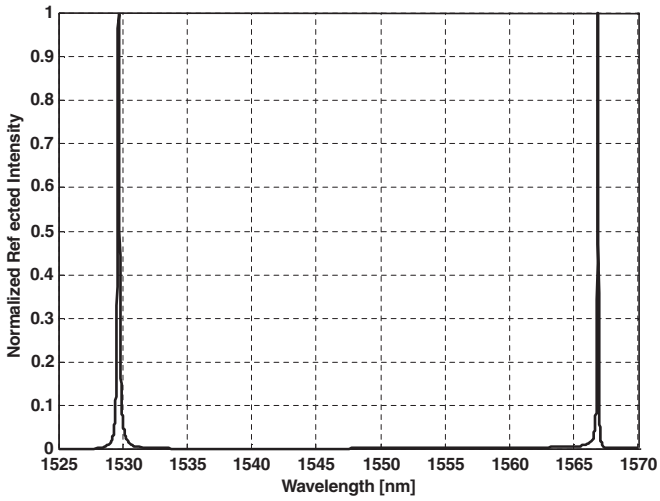

Fig. 5. Calculated normalized reflected intensity as a function of wavelength for a double-resonance GWS corresponding with intersection point B in Fig. 2. The calculated spectral resonance bandwidths at FWHM are 0.17 nm and 0.08 nm for $\lambda_1 = 1530$ nm and $\lambda_2 = 1567$ nm, respectively

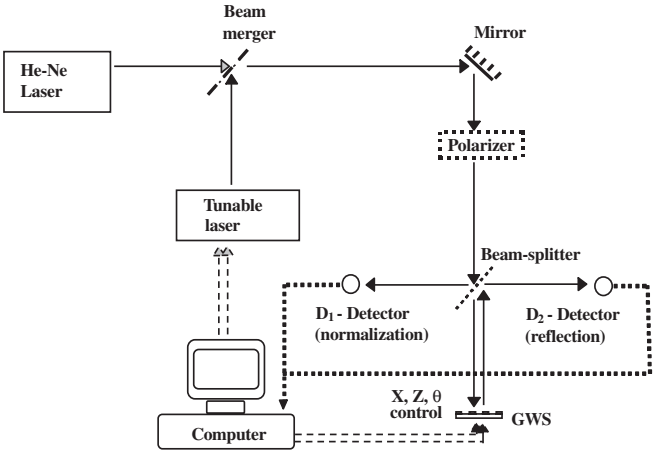

Fig. 6. Experimental arrangement to evaluate the double-resonance GWS

most entirely by the InP regrowth process, since it started at the InP buffer layer. This regrowth technique resulted in a layer structure which was as accurate as the MOCVD nominal accuracy, i.e., several atomic layers. Finally, anti-reflection (AR) coating layers were deposited on top of the uppermost layer to decrease the Fresnel reflection, so as to obtain a high contrast ratio of the on-resonance power reflection to the off-resonance power reflection. These AR layers were composed of a 121 nm layer of Al_2O_3 ($n = 1.63$ at $\lambda = 1.55\,\mu$m), and a 67 nm layer of Nb_2O_5 ($n = 2.04$ at $\lambda = 1.55\,\mu$m).

4 Experimental procedure and results

We measured and evaluated the resonance behavior of the different double-resonance GWSs that were fabricated. The experimental set-up for testing these elements is shown in Fig. 6. It included a tunable external cavity diode laser operating in the wavelength region of 1500–1590 nm. The beam from the laser, of about 4 mm^2 area, illuminated only a small part of the GWS area. The spectral resolution of the laser system was 0.003 nm. Part of the laser beam was normally incident, through a beam-splitter, on the sample, which was placed on a translating and rotating stage (sub-micron and sub-arcsecond resolutions, respectively). For normalization, part of the incident beam was reflected from the beam-splitter and monitored by a detector (D_1). The light reflected from the GWS was collected using another detector (D_2). A computer was used for controlling the wavelength of the tunable laser and the position and angle of the GWS carrying stage, as well as for monitoring all measurements from the various detectors. We used a polarizer to control the polarization of the incident light.

The experimental measurements of the normalized reflected intensity as a function of wavelength for the GWS corresponding to intersection point B in Fig. 2 and the numerical calculations of Fig. 5 are shown in Fig. 7. At the resonance wavelength $\lambda_1 = 1529.9$ nm, the normalized peak reflected

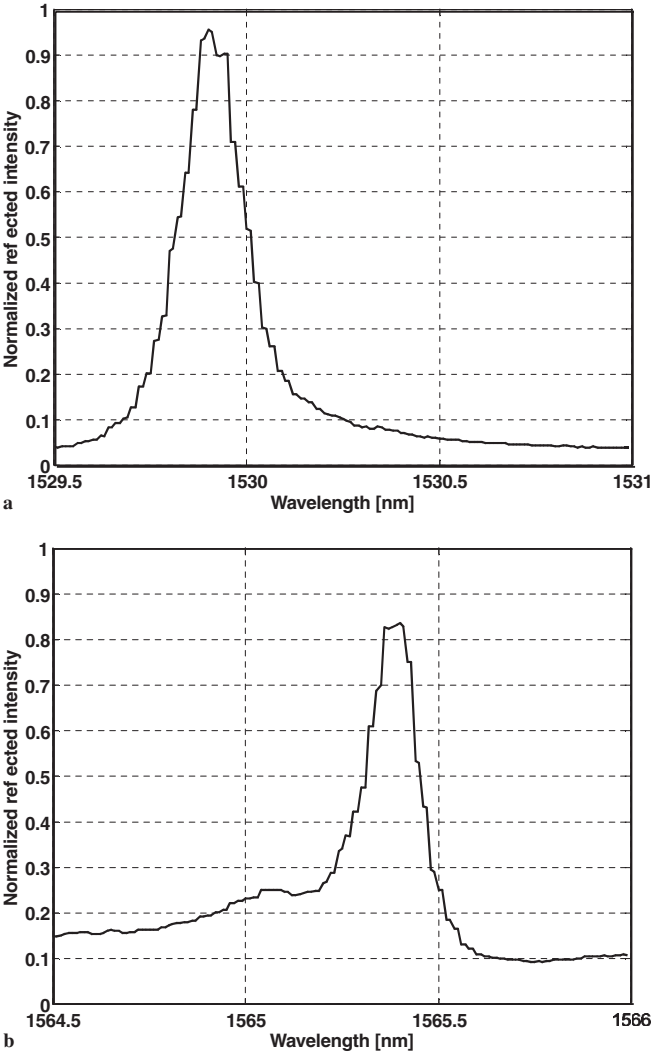

Fig. 7a,b. Experimental measurements of the spectral response of the double-resonance GWS corresponding with intersection point B in Fig. 2. **a** At the resonance wavelength $\lambda_1 = 1529.9$ nm, the spectral bandwidth is 0.2 nm at FWHM and the normalized reflected intensity is 95%; **b** At the resonance wavelength $\lambda_2 = 1565.4$ nm, the spectral bandwidth is 0.17 nm at FWHM and the normalized reflected intensity is 84%

intensity was 95%, and the spectral bandwidth at FWHM was 0.2 nm. At the resonance wavelength $\lambda_2 = 1565.4$ nm, the normalized peak reflected intensity was 84%, and the spectral bandwidth at FWHM was 0.17 nm. Thus the finesses for these resonances are about 7500 and 9000, respectively. As is evident, the experimental results are in good agreement with the predicted results shown in Fig. 5. Some asymmetry is seen in the shape of the resonances in the experimental results. We believe it is caused by the interference between the modes inside the waveguide [18]. We attribute the fact that the measured reflectivity did not reach 100% to losses in the GWS. Such losses result from three main causes: (a) nonuniformities in the thickness of the waveguide layer, introduced during the deposition process; (b) stitching errors between adjacent electron beam fields, resulting from distortions that occur during the grating exposure; and (c) light leakage from the edges of the GWS.

5 Concluding remarks

We presented here a GWS configuration that enables a tailored double-resonance wavelength response. We developed a simple first-order approximation model followed by minor higher-order corrections to perform accurate determination of the GWS parameters. Accordingly, we have designed, fabricated, and experimentally demonstrated that double spectral resonances in GWS in the 1500–1600 nm wavelength region can be achieved. Resonances with spectral bandwidths as low as 0.2 nm were achieved.

Our results clearly indicate that two simultaneous resonance wavelengths can be readily obtained from one GWS, thereby extending their range of applications, such as WDM and optical communication systems.

Acknowledgements. We would like to thank Herbert Burkhard and Bertilo E. Kempf, from the Research Department of Optoelectronics, Deutsche Telekom, Darmstadt, Germany, for helpful discussions and aid in fabricating the GWS samples. We acknowledge the support, in part, of the Israeli Ministry of Science.

References

1. R.W. Wood: Philos. Mag. **4**, 396 (1902)
2. A. Hessel, A.A. Oliner: Appl. Opt. **4**, 1275 (1965)
3. M. Neviere: *Electromagnetic Theory of Gratings*, ed. by R. Petit (Springer-Verlag, Berlin 1980) Chapt. 5
4. E. Popov, L. Mashev, D. Maystre: Opt. Acta **32**, 607 (1986)
5. S.S. Wang, R. Magnusson, J.S. Bagby, M.G. Moharam: J. Opt. Soc. Am. A **7**, 1470 (1990)
6. R. Magnusson, S.S. Wang: Appl. Phys. Lett. **61**, 1022 (1992)
7. S. Peng, G.M. Morris: Opt. Lett. **21**, 549 (1996)
8. T. Tamir, S. Zhang: J. Opt. Soc. Am. A **14**, 1607 (1997)
9. G.A. Golubenko, A.S. Svakhin, V.A. Sychugov, A.V. Tischenko: Sov. J. Quantum Electron. **15**, 886 (1985)
10. I.A. Avrutskii, G.A. Golubenko, V.A. Sychugov, A.V. Tischenko: Sov. Tech. Phys. Lett. **11**, 401 (1985)
11. I.A. Avrutskii, V.A. Sychugov: Sov. Phys. Technol. Phys. **32**, 235 (1987)
12. R. Magnusson, S.S. Wang: Proc. SPIE **2108**, 380 (1993)
13. S.S. Wang, R. Magnusson: Appl. Opt. **32**, 2606 (1993)
14. A. Sharon, D. Rosenblatt, A.A. Friesem, H.G. Weber, H. Engel, R. Steingrueber: Opt. Lett. **21**, 1564 (1996)
15. S. Tibuleac, R. Magnusson: IEEE Photo. Technol. Lett. **9**, 464 (1997)
16. A. Sharon, S. Glasberg, D. Rosenblatt, A.A. Friesem: J. Opt. Soc. Am. A **14**, 588 (1997)
17. D. Rosenblatt, A. Sharon, A.A. Friesem: IEEE J. Quantum Electron. **QE-33**, 2038 (1997)
18. S. Glasberg, A. Sharon, D. Rosenblatt, A.A. Friesem: Opt. Commun. **145**, 291 (1998)
19. A. Sharon, D. Rosenblatt, A.A. Friesem: Appl. Phys. Lett. **69**, 4154 (1997)
20. G. Levy-Yurista, A.A. Friesem: Appl. Phys. Lett. **77**, 1596 (2000)
21. P.K. Tien, R. Ulrich: J. Opt. Soc. Am. **60**, 1325 (1970)
22. P. Sheng, R.S. Stepleman, P.N. Sanda: Phys. Rev. B **26**, 2907 (1982)